MNRAS **000**, 1–?? (....) Preprint 7 February 2017 Compiled using MNRAS LATEX style file v3.0

Impact of photometric variability on age and mass determination of Young Stellar Objects: A case study on Orion Nebula Cluster

Sergio Messina[1⋆], Padmakar Parihar[2†], Elisa Distefano[1‡]
[1] *INAF-Catania Astrophysical Observatory, via S. Sofia 78, I-95123 Catania, Italy*
[2] *Indian Institute of Astrophysics, Bangalore 560034, India*

arXiv:1702.01592v1 [astro-ph.SR] 6 Feb 2017

Accepted ..... Received .....; in original form .....

ABSTRACT

In case of pre-main sequence objects, the only way to determine age and mass is by fitting theoretical isochrones on color-magnitude (alternatively luminosity-temperature) diagrams. Since young stellar objects exhibit photometric variability over wide range in magnitude and colors, the age and mass determined by fitting isochrones is expected to be inaccurate, if not erroneous. These in turn will badly affect any study carried out on age spread and process of star formation. Since we have carried out very extensive photometric observations of the Orion Nebula Cluster (ONC), we decided to use our multi-band data to explore the influence of variability in determining mass and age of cluster members. In this study, we get the amplitudes of the photometric variability in V, R, and I optical bands of a sample of 346 ONC members and use it to investigate how the variability affects the inferred masses and ages and if it alone can take account for the age spread among the ONC members reported by earlier studies. We find that members that show periodic and smooth photometric rotational modulation have their masses and ages unaffected by variability. On other hand, we found that members with periodic but very scattered photometric rotational modulation and members with irregular variability have their masses and ages significantly affected. Moreover, using Hertzsprung-Russell (HR) diagrams we find that the observed I band photometric variability can take account of only a fraction (∼50%) of the inferred age spread, whereas the V band photometric variability is large enough to mask any age spread.

Key words: stars: activity - stars: rotation - stars: pre-main-sequence - stars: Hertzsprung-Russell and colour magnitude diagrams - stars: individual: Orion Nebula Cluster

1 INTRODUCTION

Almost all Orion Nebula Cluster (ONC) members are variable stars, the amplitude of their optical photometric variability ranging from a few hundredths up to more than 1 magnitude (see, e.g., Herbst et al. 2002). Generally, classical T Tauri stars (CTTS) exhibit variability levels larger than weak line T Tauri stars (WTTS) (see, e.g., Grankin et al. 2007; Grankin et al. 2008; Herbst et al. 2000). The photometric variability manifests itself over different timescales, from minutes up to several years and they are linked with different mechanisms of variability (see, e.g., Messina et al. 2004). The photometric variability manifests itself in all photometric bands and certainly poses difficulties when we attempt to use color-magnitude diagrams (CMD) to accurately determine stellar ages and masses by means of the isochronal fitting. For a given young cluster, distribution of age of cluster members provide a tool to probe the history of star formation. The observed magnitudes and colors of young stellar objects are generally affected by either fading/reddening or brightening/blueing effects, due to magnetic stellar activity, extinction by circum-stellar disc and variable accretion phenomena arising from star-disc interaction. Due to this the observed color-magnitude can be very different from the intrinsic true values which is

⋆ E-mail: sergio.messina@oact.inaf.it
† E-mail: psp@iiap.res.in
‡ E-mail: elisa.distefano@oact.inaf.it

© .... The Authors

needed for fitting the isochrones. In the following, we show that the longer is the available photometric time series the more accurate is the determination of intrinsic magnitudes and colors, as well as of the amplitude of variability.

Measurements of I magnitudes and V−I colors for a fairly large sample of ONC members was first carried out by Hillenbrand (1997), but from snapshot observations and, consequently, with no information on variability. Time series observations in I band were subsequently carried by Herbst et al. (2002) (hereafter H02) for ONC members over a period of 45 days. Their time series allowed them to explore the range of the I-band photometric variability with time scales from hours to weeks. More recently, we collected five consecutive years of I magnitudes for a sample of 346 ONC members (Parihar et al. 2009; hereafter Paper I). The improvement in measuring the average I magnitudes and the amplitudes of variability with respect to the single season of H02 and with respect to the snapshot observations of Hillenbrand (1997) is evident in Fig. 5 of Paper I. The difference between the I band magnitude from Hillenbrand single snapshot observations and the mean I band magnitude determined by us can be up to 2 magnitudes, whereas difference with H02 can be up to 1 magnitude.

It is true that Herbst and collaborators have monitored ONC at Van Vleck Observatory (Herbst et al. 2000) in the I band during 1990-1999, therefore for a time interval much longer than ours, deriving average magnitudes and variability of amplitudes more accurately than us and for a larger sample of bright stars. However, the major improvement in our observations is that we could collect simultaneously data in three different bands (V, R, and I) and for 5 consecutive years. This puts us in a better position to derive average values to position ONC stars in CMDs and to investigate what impact the photometric variability may have on the age and mass determination.

We present the data in Sect. 2 and our analysis in Sect. 3. The effect of rotation and long-term cycles on observed magnitudes and colors are presented in Sect. 4. The modeling of color variations is presented in Sect. 5, whereas discussion and conclusions are presented in Sect. 6 and 7.

2 DATA

As described in Paper I, we have collected five seasons (from 2003-2004 to 2007-2008) of I- and V-band data and one season (2007-2008) of additional R-band data for a total of 346 ONC members. To date, this is the most complete (in terms of number of photometric bands) multi-year database of VRI observations for ONC members.

Our members belong to a $10' \times 10'$ field of view (FoV) located South-West of the Trapezium stars and whose extinction-corrected magnitudes and colours are in the range $12 \lesssim V_0 \lesssim 20$ mag and $0 \lesssim (V-I)_0 \lesssim 5$ mag, respectively. Starting from the 2008-2009 season, we have been monitoring a larger $20' \times 20'$ region to make our database more complete also in terms of members.

Our stellar sample has been observed with the 2-m Himalayan Chandra Telescope (HCT) and the 2.3-m Vainu Bappu Telescope (VBT) of the Indian Astronomical Observatory (IAO, India). On each telescope pointing, we collected 3-4 consecutive frames within very short intervals of time (< 1 hr) that were subsequently combined to compute an average magnitude and standard deviation. The standard deviation may be considered a robust estimate of the achieved photometric accuracy. More of such telescope pointings were made during each observation night. We refer the reader to Paper I for a detailed description of the observation strategy, pre-reduction process, magnitudes extraction, and data preparation.

Briefly, in order to remove possible outliers from our time series data, we applied a 3σ clipping filter. Owing to the season-to-season variation of the star's average magnitude, it turned out to be more accurate to apply such a filter to each seasonal time series rather than to the whole time series. The observation season generally lasted from two to six consecutive months and about 0.15% observations were discarded for the subsequent analysis. A fraction of such outliers may arise from intrinsic variability, likely related to flare events. However, owing to their very small percentage, their exclusion does not affect the results of our analysis. In Tables 1–3 we summarize the photometric properties of our targets in the V and I bands and in the V−I color, respectively. In the columns we list, the [PMD2009] serial number, number of observations, number of outliers, number of seasons, average magnitude V_{mean} and its standard deviation σ_{tot} computed for the complete 5-yr time series, the average seasonal standard deviation $< \sigma_{seas} >$ and the standard deviation of the seasonal mean magnitudes $\sigma_{<Vseas>}$, the brightest and faintest magnitudes in the complete time series and the photometric precision. We refer the reader to the Appendix for a description of the method used to measure the brightest/faintest magnitudes and the amplitude of variability. To make a more accurate estimate of these quantities we considered only seasons having ten or more observations for each star.

3 CAUSES OF VARIABILITY

The photometric variability of low-mass pre-main-sequence and main-sequence stars arises from a number of phenomena[1] that manifest on different time scales (see, e.g., Messina et al. 2004). The phenomenon that produces the most stable and better characterized variability is the rotational modulation of surface temperature inhomogeneities. Its time scale (i.e., the rotation period) ranges from about half a day to several days and, generally, is never longer than about 20–30 days.

Another contribution to the observed variability, in which amplitude can be larger than that arising from rotational modulation, comes from transient phenomena, like flares or extinction-related brightness fadings, and manifests on shorter time scales. Owing to its stochastic nature, it is less easily characterized.

[1] In our analysis of variability phenomena we limit to single stars and non-eclipsing binaries.

Table 1. Summary of V-band photometry of ONC members. In order of column, we list the [PMD2009] serial number, number of observations, of outliers, of seasons, the average magnitude V_{mean} and its standard deviation σ_{tot} computed for the complete 5-yr time series, the average seasonal standard deviation $< \sigma_{seas} >$ and the standard deviation of the seasonal mean magnitudes $\sigma_{<Vseas>}$, the brightest and faintest magnitude in the complete time series (see Appendix) and the photometric precision. The full table is available online.

[PMD2009] number	# obs.	# out.	# season	V_{mean} (mag)	σ_{tot} (mag)	$< \sigma_{seas} >$ (mag)	$\sigma_{<Vseas>}$ (mag)	V_{min} (mag)	V_{max} (mag)	precision (mag)
1	1	0	1	19.037	0.0	0.0	0.0	0.0	0.0	0.841
2	16	0	1	19.205	0.48	0.464	0.255	19.455	18.714	0.091
3	60	0	3	17.868	0.13	0.101	0.019	18.123	17.617	0.039
4	112	0	4	16.367	0.113	0.072	0.027	16.541	16.166	0.02
5	231	0	4	16.242	0.253	0.196	0.071	16.678	15.858	0.043
...	...	...	...	...	...	...	...	...	...	...

Table 2. Summary of I-band photometry of ONC members. The full table is available online.

PMD number	# obs.	# out.	# season	V_{mean} (mag)	σ_{Tot} (mag)	$< \sigma_{seas}$ (mag)	σ_{Vseas} (mag)	Vmin (mag)	Vmax (mag)	precision (mag)
1	334	2	4	13.944	0.126	0.099	0.04	14.283	13.794	0.026
2	238	0	5	17.545	0.383	0.322	0.067	18.272	16.822	0.052
3	320	0	5	15.004	0.038	0.035	0.01	15.065	14.931	0.017
4	310	0	5	13.421	0.079	0.044	0.013	13.586	13.293	0.011
5	558	3	5	14.318	0.207	0.19	0.081	15.078	13.972	0.029
...	...	...	...	...	...	...	...	...	...	...

Table 3. Summary of V−I photometry of ONC members. The full table is available online.

PMD number	# obs.	# out.	# season	V_{mean} (mag)	σ_{Tot} (mag)	$< \sigma_{seas}$ (mag)	σ_{Vseas} (mag)	Vmin (mag)	Vmax (mag)	precision (mag)
1	2	0	0	5.041	0.0	0.0	0.0	5.041	5.041	0.841
2	36	0	1	1.968	0.532	0.0	0.0	3.109	0.891	0.095
3	66	0	3	2.875	0.126	0.0	0.0	3.136	2.591	0.041
4	98	0	4	2.932	0.158	0.0	0.0	3.162	2.673	0.022
5	213	0	4	1.872	0.29	0.0	0.0	2.239	1.125	0.05
...	...	...	...	...	...	...	...	...	...	...

Active region growth and decay (ARGD), variable accretion, and activity cycles also contribute to the photometric variability on the longest time scales, from several weeks the first to several years the latter. Characterization of such variability requires multi-year monitoring. Every cause of variability has a spectrum of amplitudes whose range can be accurately determined if the photometric time series is much longer than the characteristic time scales, i.e., if the phenomenon producing the variability is sampled over sufficiently longer periods

In our study, we can state that our 5-yr long monitoring is best suited to characterize the amplitude of variability arising from both rotational modulation and ARGD. Whereas, observational sampling more frequent and uninterrupted than ours is required to make a robust statistics of stochastic phenomena. To some extent our observations allow us to detect these phenomena, but certainly not their complete amplitude spectrum. Finally, activity cycles and other long-term activities manifest them self over the periods from few years to decades. Therefore, we can derive only lower limits to amplitudes of long term variability.

As a matter of fact, the longer the time series the better the characterization of the whole spectrum of variability. In Fig. 1, we show, as an example for the V and I bands, how the level of observed variability, and therefore the capability of detecting the complete amplitude spectrum, increases as time series lengthens. In the same figure we show for each target the V band (left) and I band (right) standard deviation versus mean magnitude considering the last observation season to begin, that is observations collected in 2007-2008 (green triangles), which is our longest observation season, and overplot its lower envelope (green solid line). This envelope is computed averaging the 10% smallest values within each bin of one-magnitude width. Then, we consider the standard deviation from the last two years of observations (sky-blue crosses), and so on. Finally, we consider the σ_{tot} (red bullets) of the complete time series.

It is evident that as far as the series becomes longer, the variability amplitude, as measured by the standard deviation, tends to increase. This happens because we are

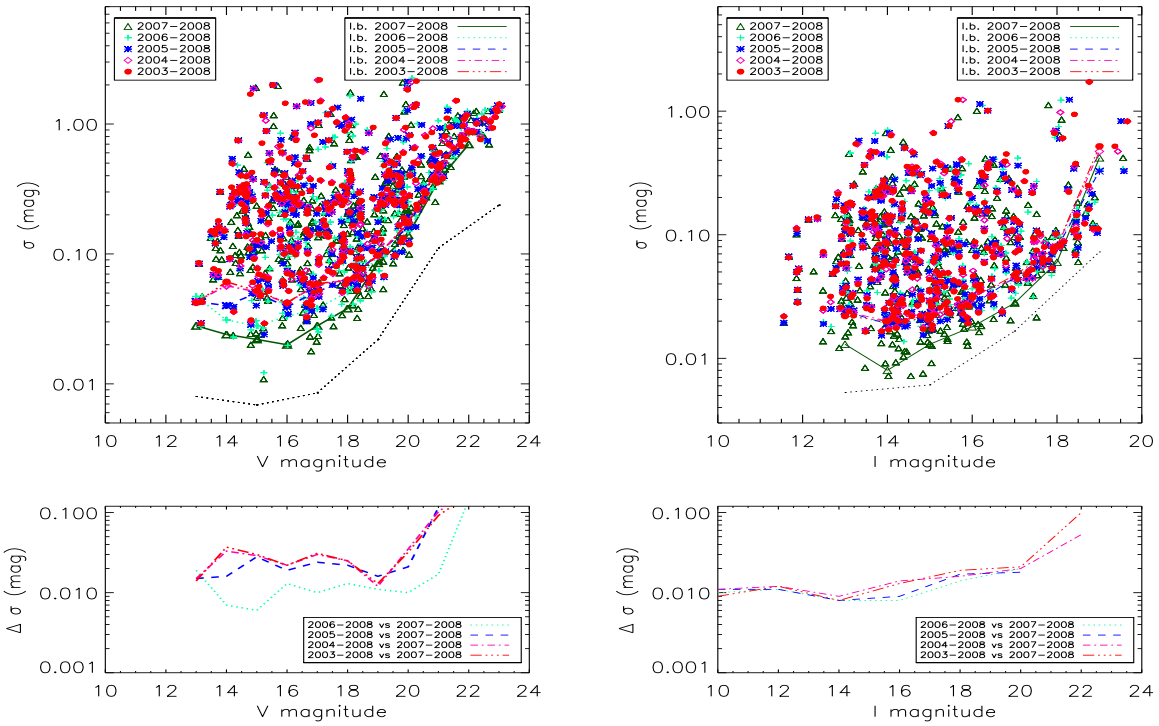

Figure 1. Top panels: standard deviation (σ) versus mean magnitude (left for V band and right for I band) for the complete sample of ONC members computed considering time intervals of increasing length. The lines represent the corresponding lower envelopes of the σ distributions. The black dotted line represents the photometric precision. Bottom panels: differences between the lower envelopes computed considering time intervals of increasing length with respect to the last observation season (2007-2008).

obtaining a more accurate estimation of all variability components. As shown in the lower panels of Fig. 1, the largest increase is obtained when we add a second consecutive season of observations, and again a third. Starting from the fourth consecutive season, the lower envelope continues to increase but at much smaller rate. In the case of the I band observations, we see a similar behavior, although the variability in the I band is smaller than in the V band and the standard deviation lower envelope increases less rapidly than in the case of V band.

We find that the ONC members exhibit a photometric variability whose average seasonal standard deviation corrected for the photometric accuracy (dotted black lines in the top panels of Fig. 1) is $< \sigma_{seas\_V} > = 0.24$ mag and $< \sigma_{seas\_I} > = 0.12$ mag, whereas the total standard deviation (on a 5-yr base line) is $< \sigma_{tot\_V} > = 0.39$ mag and $< \sigma_{tot\_I} > = 0.17$ mag. The average amplitude of variability is smaller in I band than in V, which is expected for PMS objects. The use of I band allows us to deal with photometric variability a factor of 2 smaller than V band and hence preferable in positioning the ONC members in CMDs.

To investigate any dependence of the variability level on stellar mass, we have to correct our mean magnitudes for interstellar extinction. Unfortunately, we have values of extinction (A_v) for only about 25% of our sample, specifically only for the brighter members. Using the Hillenbrand (1997) A_v values (see Sect. 3.3) to correct the magnitudes for reddening, we find that the average variability levels are $< \sigma_{tot\_V} > = 0.24$ mag and $< \sigma_{seas\_V} > = 0.12$ mag ($< \sigma_{tot\_I} > = 0.12$ mag and $< \sigma_{seas\_I} > = 0.09$ mag) in the $10 < V_0 < 15$ mag range (i.e. stars with M > 0.3-0.4 $M_\odot$) .

We plot these results in the top panels of Fig. 2, using asterisks to represent σ_{tot}, open bullets and squares to represent the average values of σ_{tot} and of $< \sigma_{seas} >$ (obtained using a binning width of 2-mag). In the bottom panels of Fig. 2, we plot the ratio of these quantities versus magnitude. We find that the average ratios are 2.0 and 1.4 for the V and I bands, respectively, and no significant dependence with mass is found.

In the following sub-sections we show that when we consider the contribution to variability arising only from periodic phenomena, that is the light rotational modulation due to surface temperature inhomogeneities, then its impact on mass and age estimation is negligible. On the other hand, when we consider the additional contribution of other non-periodic phenomena, e.g., related to variable accretion or ARGD, then the impact of variability becomes increasingly significant. The best approach to disentangle the contribution on variability by rotational modulation of temperature

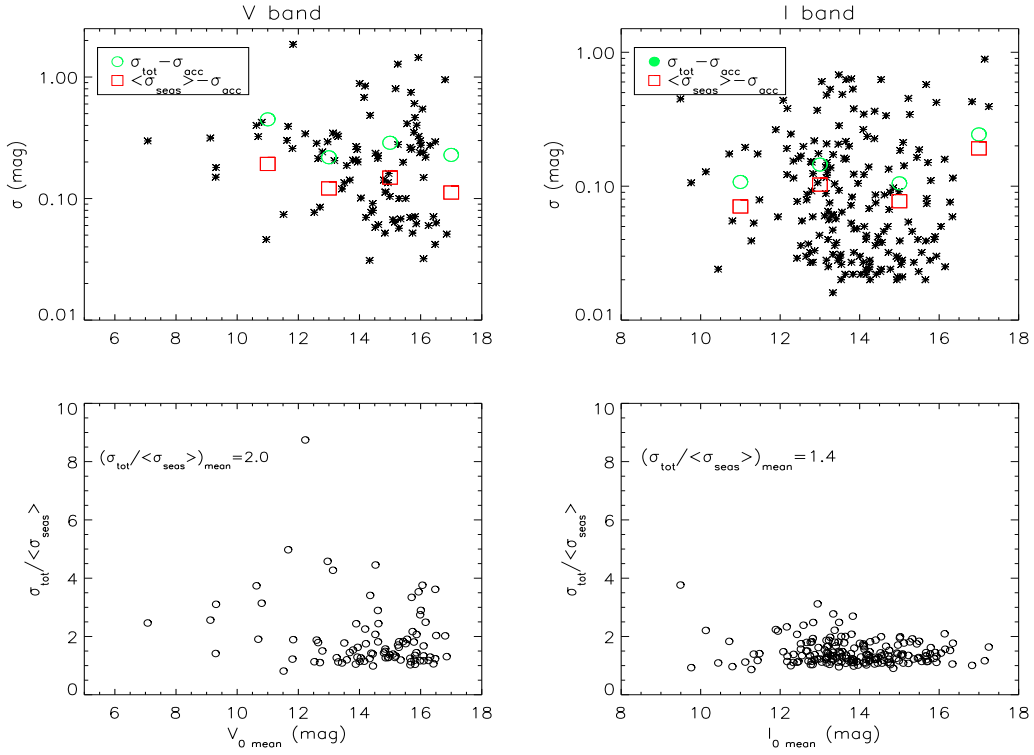

Figure 2. Top panels: total standard deviation $\sigma_{\rm tot}$ (asterisks) vs. reddening-corrected mean magnitude for V (left) and I bands (right). Open circle and squares represent the average values, computed within bins of 2-mag width, of $\sigma_{\rm tot}$ and $< \sigma_{\rm seas} >$, both corrected for the photometric precision $\sigma_{\rm acc}$. Bottom panels: ratio between $\sigma_{\rm tot}$ and $< \sigma_{\rm seas} >$ vs. reddening-corrected mean magnitude.

inhomogeneities to others is to analyze separately periodic and non periodic variables.

3.1 The samples of 'clean' and 'dirty' light curves

One major difficulty in estimating the amplitude of the rotation-induced variability from time series data is the presence of possible outliers, which can provide incorrect average magnitude, but more specifically incorrect brightest and faintest values, thus overestimating the amplitude of variability. The contribution of ARGD and activity cycles is minimized by segmenting the 5-yr long time series into segments each corresponding to the yearly observation season.

Periodic variables are best suited to identify and remove outliers, allowing us to measure more confidently the correct amplitude of rotation induced variability. In fact, once the time series data of the periodic stars are phased into folded light curves, it becomes quite easy to identify any data that significantly deviates from the trend caused by the rotational modulation. These outliers can arise either from bad measurements or from the above mentioned transient phenomena that are likely unrelated to the rotational modulation.

We know the rotation periods of 165 of the 346 stars considered in the present analysis. The rotation periods of 55 stars were discovered by us (Paper I), 17 stars by Rodríguez-Ledesma et al. (2009), whereas remaining 93 stars were reported as periodic variables in the literature (e.g., Herbst et al. 2000, 2002; Stassun et al. 1999).

We have produced phased light curves of all 165 periodic stars. Then, we have automatically removed from each light curve all data deviating more than 3σ from the mean value, and any other remaining observation that with visual inspection appeared to significantly deviate from the sinusoidal trend imposed by the rotational modulation.

After cleaning the phased light curves from outliers, we have selected a subsample consisting of very smooth light curves. These are light curves that were best fitted by a single sinusoidal function and whose ratio (R) between the amplitude and the average residuals from the fit was arbitrarily set to be $R \geqslant 2.5$. Since these smooth light curves also exhibit some level of magnitude dispersion at any given rotation phase, in the following we adopt the brightest and faintest values of the sinusoidal fit as the brightest and faintest light curve values. For an example in Fig. 3 we show a very smooth light curve of the star [PMD2009] 311 in the 2007-2008 season. The top-left panels display the I, R, and V magnitudes and the top-right panels display the V−I, R−I, and V−R color curves phased with the rotation period P = 9.89 d taken from Paper I. The solid blue lines are the sinusoidal fits to the data with the rotation period. In the bottom panels we plot the magnitude vs. color and color vs. color distributions, which are linearly fitted (red solid line) and for which the Pearson linear correlation coefficients and significance levels are computed. The slope provide a valuable

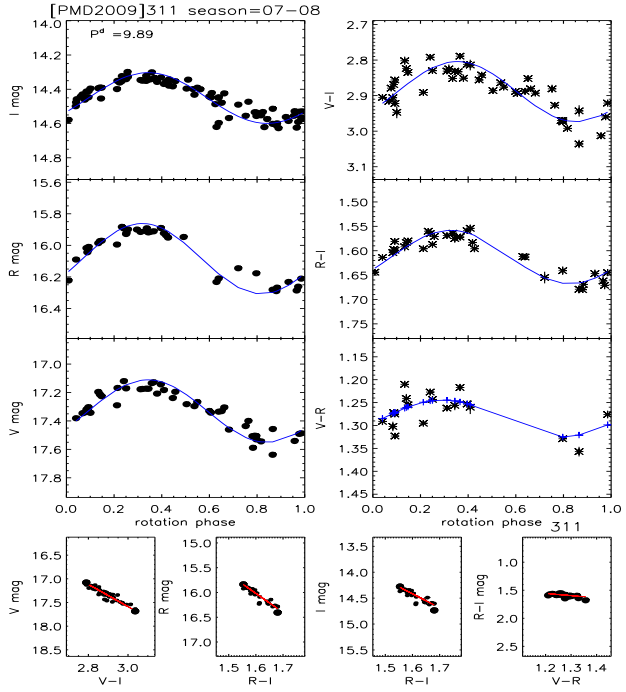

Figure 3. Example of 'clean' magnitude and color curves (top panels) of the star [PMD2009] 311 in the season 2007-2008. Data are folded with the rotation period and fitted with a single sinusoidal function (solid line). The magnitude vs. color and color vs color distributions are plotted in the botton panels together with a linear fit (solid line).

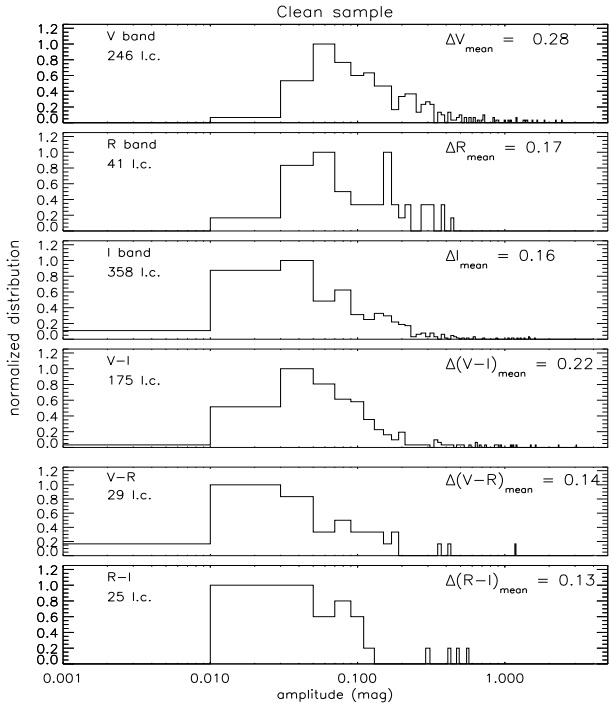

Figure 4. Normalized distributions of light and color curve amplitudes from the clean sample. Labels indicate the number of curves (l.c.) used to build the distributions.

information on the average temperature contrast of the surface inhomogeneities with respect to the unperturbed photosphere. These slopes can change from star to star, and for the same star can change from season to season.

Using the R value as criterion to distinguish light curves, we were left with one sub-sample of very smooth light curves (hereafter named 'clean' periodic) with $R \geqslant 2.5$ and one sub-sample of quite scattered light curves (hereafter named 'dirty' periodic) with $1.0 \leqslant R < 2.5$. Stars with R < 1, although have their rotation period known from the literature, show no light rotational modulation in our time series.

We remind that each periodic star has up to 5 light curves in the I and up to 5 in the V bands (since the complete time series is analyzed after splitting into 5 consecutive seasons), whereas it has only one light curve in R band, which is available for the 2007-2008 season. We find that each star during the same season can have either all light curves (V, I, V−I) clean or all dirty, or a combination in which light curve changed from one season to other season and dirty became clean or visa versa.

In general, dirty light curves are more numerous than the clean ones. On a total of 797 I-band light curves, 45% are clean; on a total of 156 R-band light curves, 26% are clean; on a total of 800 V-band light curves, 31% are clean. If we consider that about 50% of the complete stellar sample (346 stars) is made by non periodic stars (whose time series can be considered as dirty), then we derive that among ONC members clean light curves are found with a percentage never larger than 25% in the I band, and never larger than 15% in the V band. As extreme cases we mention the following stars: [PMD2009] 57, 147, 182, 191, 256, 274, 311, 333 whose light curves are all and always clean, whereas the following stars: [PMD2009] 23, 98, 100, 132, 185, 192, 224, 227, 334, 337 have all and always dirty light curves.

In Fig.4, we plot the normalized distributions of the magnitude and color curves amplitudes for the 'clean' sample on a logarithmic scale. Labels report the number of light curves (l.c.) used to build the distributions, and the average peak-to-peak light curve amplitude. On average, the V light curves have amplitudes larger than R and I light curves, and the V−I color curves have amplitudes larger than V−R and R−I. Such a trend is consistent with variability arising from temperature inhomogeneities (either hotter or cooler than the unperturbed photosphere) carried in and out of view by the stellar rotation. We note that there are some V-band light curves having amplitudes larger than 0.5 mag. Generally, among pre-main-sequence weak-line T Tauri stars or main-sequence stars, whose photometric variability is dominated by cool spots, amplitudes are not larger than 0.5 mag (see, e.g., Messina et al. 2001, 2010, 2011). Nonetheless, exceptions exists, like the T Tauri star V410 Tau for which light curve amplitudes up to $\Delta V = 0.7$ mag are been measured (e.g., Oláh et al. 2009).Our detection of larger amplitudes in a few stars then may suggest that also hot spots on the stellar photosphere created by disk accretion may be present in our clean star sample.

3.2 CMD for 'clean' periodic light curves

To compare our observations with theoretical isochrones in CMDs, we have to remove the effect of reddening from our measurements. We have at our disposal the works by Hillenbrand (1997) and, more recently, by Da Rio et al. (2010) in which the reddening of numerous ONC members is computed. In the first work, we find measured reddening A_V for 108 out of 165 periodic stars, in the second case for 97 out of 165. Hillenbrand (1997) and Da Rio et al. (2010) use different methods to estimate A_V, and for our periodic stars in common to both studies, their estimate differ on average by A_{V_Hill}-A_{V_DaRio}=−0.93 mag (with differences ranging from −3.9 mag to 1.3 mag). In the following analysis, we use only a sub-sample of 'clean' light curves with known extinction to build our CMDs, whereas in Sect. 5 we can use the complete sample to investigate the slopes of the magnitude vs. color variations (which are independent from extinction). In order to have homogeneity in the data, we have used A_V determined by Hillenbrand only, which provided us a larger sample of extinction-corrected light curves.

In the left panel of Fig. 5 we plot, in the form of segments, the intrinsic V_0 magnitude and $(V-I)_0$ color variations derived from the clean sample of light curves. We find that all V_0 vs. $(V-I)_0$ variations (line segments in CMD) have correlation coefficient with significance level larger than 95%. We use black, red, and green colors to distinguish V_0 vs. $(V-I)_0$ variations with correlation coefficient $r > 0.95$, $0.90 < r < 0.95$, and $r < 0.90$, respectively. For instance, two or more segments may refer to the same star, but corresponding to different seasons. We overplot the isochrones for 0.1, 1 and 10 Myr, and the zero-age-main-sequence (ZAMS; solid red lines) computed according to the Siess et al. (2000) models for solar metallicity. We also plot evolutionary mass tracks (dotted blue lines) for different mass values in the range of 0.1–1.5 $M_\odot$.

The slopes $\Delta V_0/\Delta(V-I)_0$ exhibit a range of values whose mean and median values are 2.35 and 2.17, respectively (see top right panel). Moreover, the slopes appear to decrease at increasing color (decreasing mass). We found similar results when data are analysed separatedly, according to the correlation coefficient values ($r > 0.95$, $0.90 < r < 0.95$, and $r < 0.90$).

A comparison with a family of isochrones from Siess et al. (2000) (at s.pdf of 1 Myr) allows us to estimate the age of our targets. Specifically, we infer two different ages from each light curve, one corresponding to the light curve brightest/bluest value, and another to the faintest/reddest value. The difference between the two inferred ages provides us with an estimate of the impact of variability, arising from rotational modulation of temperature inhomogeneities, on the age estimate of that star within the same observation season. Since, from season to season the position of the targets (represented by a segment in the CMD) can change owing to AR evolution, then our results represent the only effects of rotational modulation. From visual inspection of Fig. 5 it is clearly evident that on average the presence of surface inhomogeneities on the stellar surface induces magnitude and color variations whose slope is similar to that of the isochrones in the CMD. It means that variability will not have significant impact on the age determination. Nonetheless, we can compute the age of our stars and the results are plotted in the panels of Fig. 6. Here, we plot using solid lines the distribution of ages derived from brightest/bluest values (top panel) from faintest/reddest values (middle panel), and their differences, that is ages from faintest minus ages from brightest (bottom panel). We find that the derived oldest and youngest mean ages are about the same (2.7 and 2.6 Myr, respectively) and the age difference is found to be 0.1 Myr which is not very significant. Nonetheless, we found in about 10% cases activity-induced apparent age difference is larger than 1 Myr (up to 8 Myr). We stress that our aim is not to compute an absolute age of the ONC members, rather to estimate the age dependency on photometric variability. This is the reason why our analysis does not require different evolutionary models.

Similarly, we can derive the mass of our targets by comparison with a family of mass evolutionary tracks (at s.pdf of 0.1 $M_\odot$). Again, we derive two mass values for each light curve corresponding to the brightest/bluest and the faintest/reddest values. The results are plotted in Fig. 7, where we show the distribution of masses derived from brightest/bluest (top panel), faintest/reddest (middle panel), and their difference (bottom panel). The derived mean values of stellar mass are found to be 0.46 $M_\odot$, 0.50 $M_\odot$, and 0.04 $M_\odot$, respectively. Again, the difference in the derived masses are smaller than the precision associated with the determination of mass from the CMD (i.e., the 0.1$M_\odot$ step). Nonetheless, in about 4% of cases the mass difference is larger than 0.1 $M_\odot$. We note in Fig. 5 that the sensitivity of mass versus V−I color variations decreases as we go toward lower masses: a mass difference of 0.1 $M_\odot$ is accompanied by a color variation of $\Delta(V-I) = 0.01$ mag at $M = 1\,M_\odot$ and $\Delta(V-I) = 0.1$ mag at about $M = 0.2\,M_\odot$. Therefore, although the bottom right region of the CMD is populated by longer segments, the corresponding mass variation is not larger at all.

We have carried out a similar analysis (see Fig. 8) for the intrinsic I_0 vs. $(V-I)_0$ variations and as expected obtained similar results. Likewise previous finding, the activity-induced apparent age differences derived in 10% of light curves are larger than 1 Myr.

We conclude that if all ONC members were periodic variable and all light curves smooth, then, the impact of photometric variability on the determination of average age would be negligible, and CMDs would be well suited to infer both mass and age. Only a fraction (10%) of stars may have their age and mass significantly affected by the photometric variability. However, as already mentioned only 50% of ONC stars in our small sample are periodic and in total only 25% have smooth light curves. Therefore, it is important to see what role the variability plays in the remaining targets.

3.3 CMD for 'dirty' periodic light curves

We make an attempt to extend our analysis to the periodic 'dirty' sample. Owing to the large scatter of the phased light curves we have taken more care to measure the brightest/faintest values and, therefore, the variability amplitude. In the Appendix, we provide a detailed discussion on the approach adopted to measure these quantities.

Once determined the amplitude of the periodic 'dirty' light curves, we can build a CMD and use it to estimate the ages and masses corresponding to the brightest/bluest and

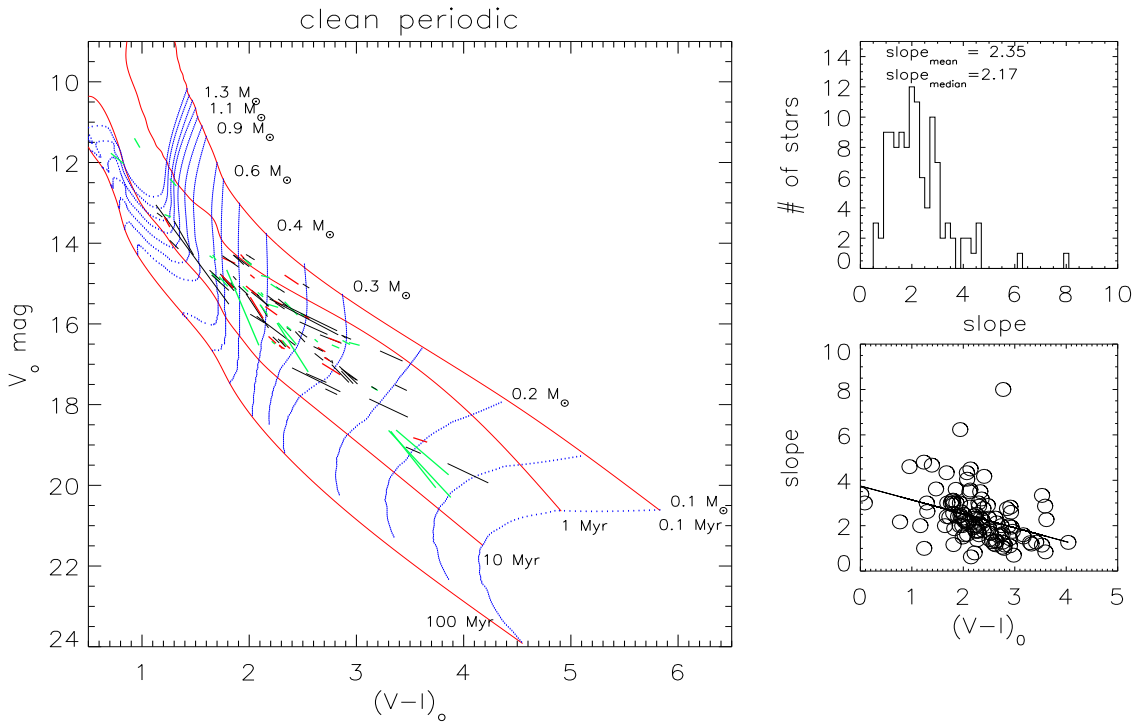

Figure 5. Left panel: V_0 vs. $(V-I)_0$ diagram for the sample of 'clean' light curves. Red solid lines and blue dotted lines represents theoretical isochrones and mass tracks from Siess et al. (2000). Black, green, and red segments indicate different degrees of correlation ($r > 0.95$, $0.90 < r < 0.95$, and $r < 0.90$, respectively). Top right panel: distribution of slope of V_0 vs. $(V-I)_0$ variations, and (bottom right panel) of slope vs. $(V-I)_0$ color.

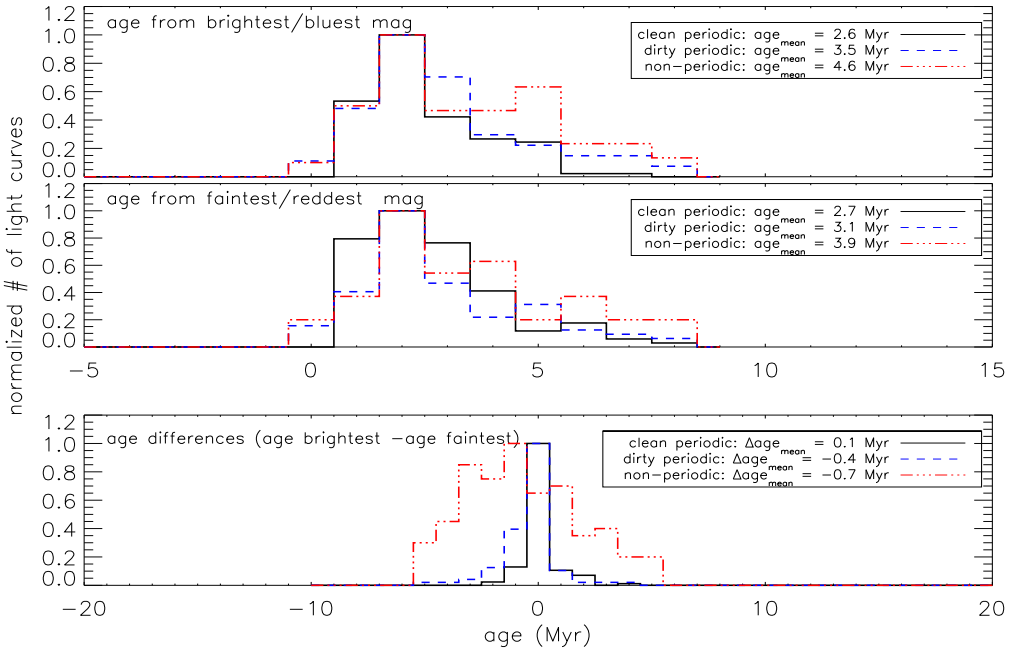
age from brightest/bluest mag
clean periodic: age_mean = 2.6 Myr
dirty periodic: age_mean = 3.5 Myr
non−periodic: age_mean = 4.6 Myr
age from faintest/reddest mag
clean periodic: age_mean = 2.7 Myr
dirty periodic: age_mean = 3.1 Myr
non−periodic: age_mean = 3.9 Myr
normalized # of light curves
age differences (age brightest −age faintest)
clean periodic: Δage_mean = 0.1 Myr
dirty periodic: Δage_mean = −0.4 Myr
non−periodic: Δage_mean = −0.7 Myr
age (Myr)

Figure 6. Distribution of ages for ONC members for 'clean' period (black solid line), 'dirty' periodic (red dashed line), and non-periodic (blue dotted-dashed line) derived from the brightest/bluest magnitude (top panel) and faintest/reddest magnitude (middle panel), and their difference (bottom panel).

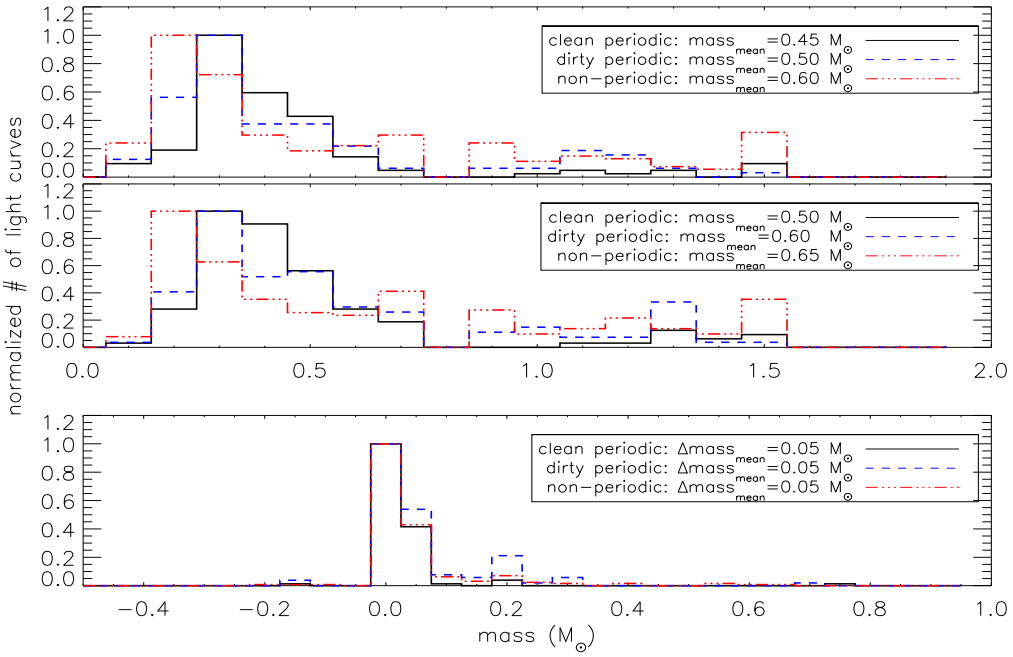

Figure 7. Distribution of masses for ONC members for 'clean' period (black solid line), 'dirty' periodic (blue dashed line), and non-periodic (red dotted-dashed line) derived from the brightest/bluest magnitude (top panel) and faintest/reddest magnitude (middle panel), and their difference (bottom panel).

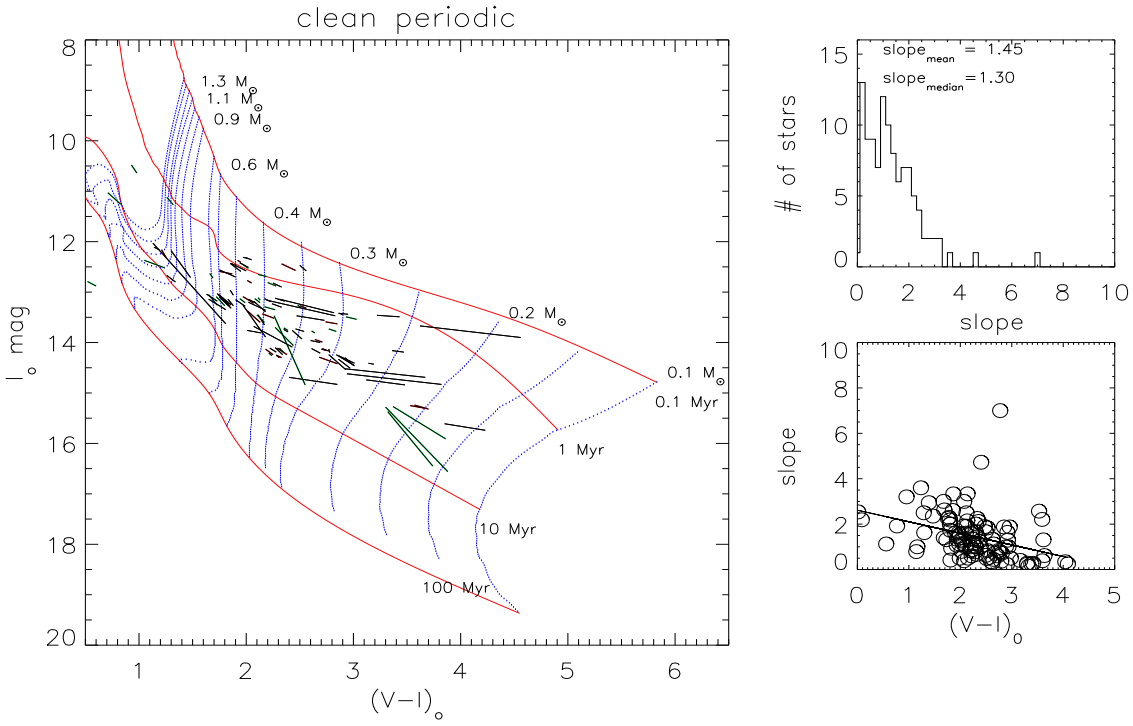

Figure 8. Same as in Fig. 5, but for I_0 vs. $(V-I)_0$

faintest/reddest values, as we carried out for 'clean' sample. The results are plotted in Fig. 9, where we have selected only light curves where the magnitude and color variations are correlated with a significance level larger than 90%.

We note a few relevant differences. First, all stars have correlation coefficients $r < 0.90$. Second, a number of stars appear in regions of the CMD where no stars are expected, that is a few stars are either too blue to be PMS stars or too red to be older than about 1 Myr. Finally, the average slope of the V_0 vs. $(V-I)_0$ relation is smaller than in the 'clean' sample, and has an average value $< \Delta V_0/\Delta(V-I)_0 > = 1.9$ (see top-right panel of Fig. 9). This means that the dirty periodic stars seem to exhibit either larger color variations or smaller magnitude variations with respect to clean periodic stars. Since the average V_0 vs. $(V-I)_0$ variation is less steep than the isochrones, therefore, age derived from the faintest value will make star to appear younger than age derived from the brightest value.

In our analysis, if we also consider the light curves whose correlation coefficients have significance level smaller than 90%, we find that the average slope is even smaller ($< \Delta V_0/\Delta(V-I)_0 > = 1.35$).

As done for 'clean' light curves, in Fig. 6 and Fig. 7, we plot the distribution of ages and masses inferred from the CMD by comparing brightest/bluest and faintest/reddest values with isochrones and evolutionary mass tracks, using dashed blue lines. We find 10% stars with age older than 10 Myr, and excluding these stars, the average age is 3.5 Myr and 3.1 Myr (from brightest and faintest magnitudes, respectively). The average difference between the age from brightest and faintest is still insignificant, although larger than in the case of 'clean' stars, that is -0.4 Myr against 0.1 Myr. However, the percentage of stars with age difference larger than 1 Myr has increased up to 20% (with respect to the 10% of 'clean' stars). Therefore, when we consider the dominant variability component due to temperature inhomogeneities together with the additional secondary component arising from either variable accretion or ARGD or stochastic events like micro-flares, then the average age appears to be older (3.2 Myr against 2.7 Myr of clean periodic stars) as well as the percentage of stars whose age estimate is significantly affected by the variability increases up to 20%. The average age is still older when we consider stars that exhibit periodic light curves but with not much tight correlation between magnitude and color variations (significance level smaller than 90%). Concerning the mass, we find the average values $0.5\,M_\odot$ and $0.60\,M_\odot$ from brightest/bluest magnitude and faintest/reddest magnitudes, respectively, and an average difference of $0.04\,M_\odot$. Again, this differences are smaller than the precision associated to our mass determination.

3.4 CMD for dirty non-periodic stars

We consider now the sample consisting of non periodic stars whose light curves can be assimilated to 'dirty' light curves. In Fig. 10 we plot the color-magnitude diagram as well as the distribution of slopes and their trend with $(V-I)_0$ color as done in the previous cases. We see that the average slope of V_0 vs. $(V-I)_0$ is $< \Delta V_0/\Delta(V-I)_0 > = 1.48$, similar to that one obtained for 'dirty' stars with un-correlated color/magnitude variations. In Fig 6, we plot the distribution of inferred ages. Excluding stars older than 10 Myr, which now represent about 50% of the sample, we find that the age from brightest magnitude is 4.6 Myr, from faintest magnitudes is 3.9 Myr, and their difference is now -0.7 mag.

Concerning the mass, we find the average values $0.6\,M_\odot$ and $0.65\,M_\odot$ from brightest/bluest magnitude and faintest/reddest magnitudes, respectively, and an average difference of and $0.05\,M_\odot$. Again, the differences are smaller than the precision associated to our mass determination. From our analysis we found that the average age of stars progressively increases from stars showing photometric variability, clean periodic (primarily due to cool spots) to dirty periodic (due to a combination of cool and hot spots) to 'irregular' photometric variability (dominated by accretion/stochastic phenomena). Furthermore, we found the irregular variables to have different ages derived from brightest and faintest magnitudes, whereas clean periodic star age is unaffected by variability. We can conclude by stating that, assuming all members are coeval, irregular photometric variability makes the stars to be appeared older and derived ages increase with amplitude of variability.

4 ROTATION + LONGTERM VARIABILITY

The analysis carried out in the previous sections considers the effect of seasonal photometric variability on determination of stellar age and the mass arising from rotational modulation of light due to temperature inhomogeneities plus any additional random component. However, owing to ARGD and activity cycles the brightest and faintest light curve values of the same star can change from season to season. Therefore, in this section we have selected those clean stars which have smooth light curves over at least two observation seasons and have plotted their magnitudes and the colors in the CMD as segment connecting the brightest/bluest and faintest/reddest values ever observed. In this way, we consider the additional component in amplitude related to long-term variability. However, limited data set collected over only 5 years may not be enough to capture the complete range of variability linked with fairly long-term trend. Therefore, our finding on the impact of variability in the age and mass determination may be taken with some caution.

We find that the average difference between ages derived from brightest and faintest values is about zero. However, the most relevant result is that the fraction of stars with differences larger that 1 Myr is now increased from 10% (when only rotational variability was considered) to about 30%.

5 SLOPE MODELLING

An important information that we can derive from our multi-band monitoring is the dependency of magnitude versus color variations, which depends on the contrast of temperature between the spotted and the surrounding unspotted photosphere. Here, again we analyze separately the clean and dirty samples. In the top-right panel of Fig. 5, we plot

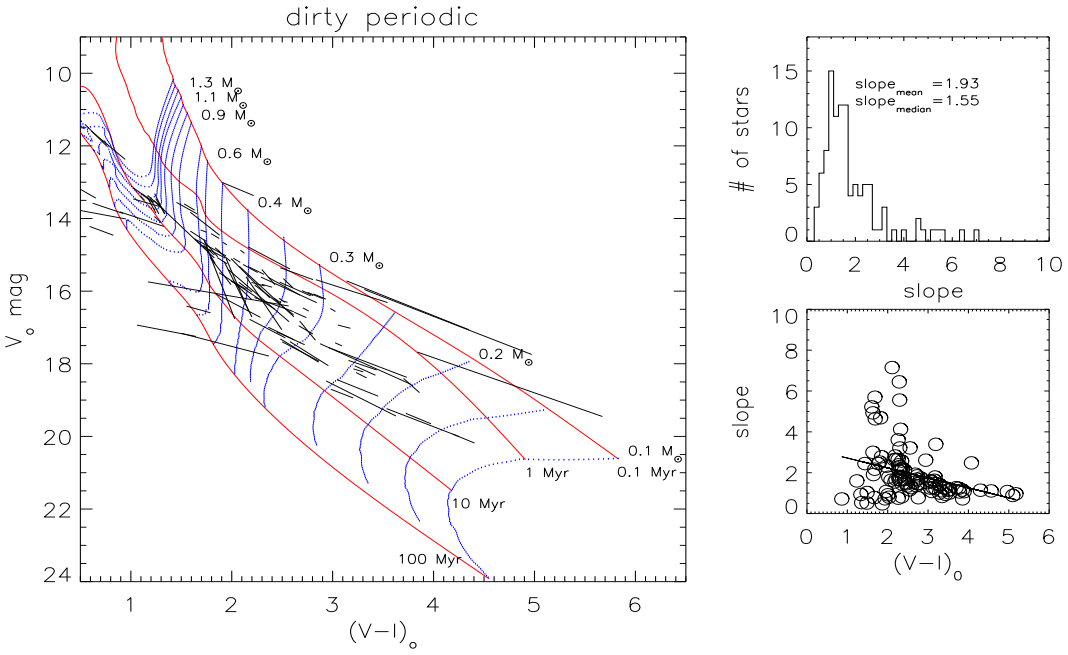

Figure 9. Left panel: V_0 vs. $(V-I)_0$ diagram for the sample of 'dirty' light curves. Top right panel: distribution of slope of V_0 vs. $(V-I)_0$ variations, and (bottom right panel) vs. $(V-I)_0$ color.

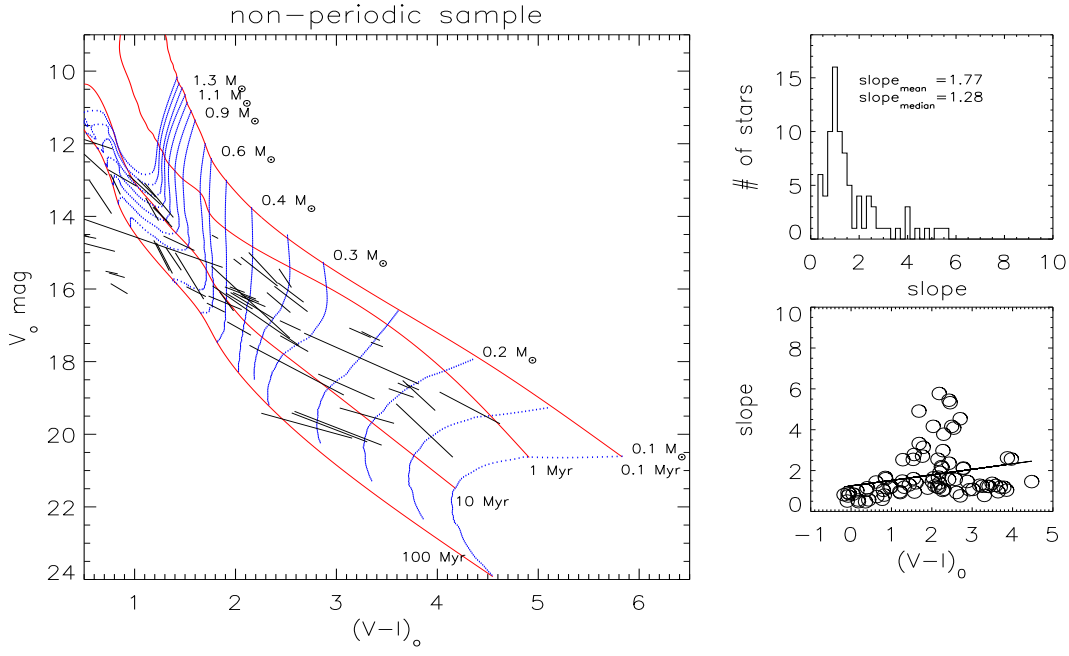

Figure 10. Left panel: V_0 vs. $(V-I)_0$ diagram for the sample of non-periodic stars. Top right panel: distribution of slope of V_0 vs. $(V-I)_0$ variations, and (bottom right panel) vs. $(V-I)_0$ color.

the distributions of slopes derived from the linear fit of V magnitude versus V−I color variations for the clean sample; whereas in top-right panel of Fig. 9 and of Fig. 10 we plot similar distributions for the dirty periodic and non periodic samples. We note that the average derived slopes for the dirty periodic light curves (2.35) and irregular variables (1.77) are smaller than the slopes derived for clean periodic stars.

Table 4. Summary of slopes and correlation coefficients of magnitude and color variation among different photometric bands. The full table is available online.

[PMD2009]	season	HJD_{mean}	N_I	N_R	N_V	b_{V_VI}	r_{V_VI}	b_{R_RI}	r_{R_RI}	b_{V_VR}	r_{V_VR}	b_{RI_VR}	r_{RI_VR}
...	...	...	...	...	...	...	...	...	...	...	...	....	....
22	06-07	2454443.8013	76	33	38	2.748	0.486	1.777	0.895	0.371	0.824	-0.581	0.57
25	06-07	2454443.8013	77	34	43	0.996	0.984	0.908	0.708	0.982	0.994	-0.014	0.627
26	06-07	2454443.8013	79	34	39	0.938	0.96	-0.530	0.665	0.966	0.994	0.226	0.64
...	...	...	...	...	...	...	...	...	...	...	...	....	....

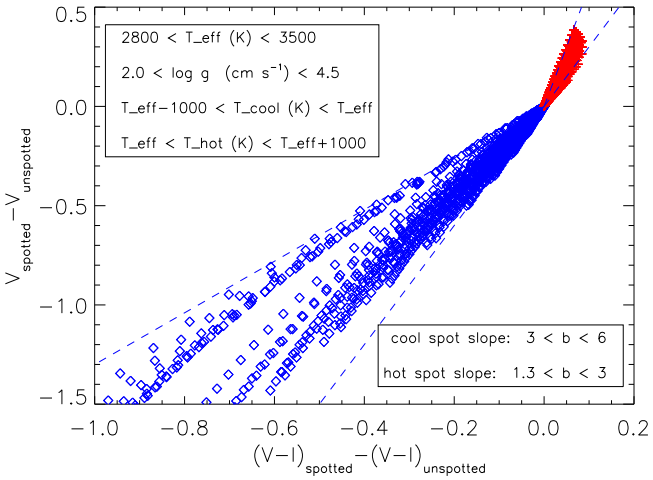

Figure 11. Model magnitude versus color variations for a range of values of effective temperature, temperature contrast between perturbed and unperturbed photosphere and surface gravity.

5.1 Correlation analysis

Magnitudes and colors of ONC stars are affected by both the presence of magnetic activity and star-disk interaction effects. In order to position our stars in color-magnitude diagrams we should use both unperturbed magnitudes and colors (or values properly corrected for the activity/accretion effects at least). If only cool spots were present on the stellar surface, then the brightest magnitude and bluest color could be presumably considered intrinsic values linked with immaculate star. This circumstance may possibly apply to most WTTS that are expected to lack accretion hot spots. However, also in WTTS there may be presence of hot faculae of magnetic origin which can make the star bluer, making the brightest values not corresponding to an unperturbed level. Moreover, in the case of binary systems with two components of different effective temperatures, when the more active and later-type star becomes fainter, owing to its variable activity, then the whole system becomes bluer (see, e.g. Messina 2008). On the other hand, if only hot spots were present on the stellar surface, then the faintest magnitude and reddest color could be assumed as 'unspotted' values (see, Messina et al. 2016). Both regression and correlation analyses between magnitude and colors can allow us to better understand the patterns of color variation of ONC stars and better investigate the nature of surface inhomogeneities.

5.2 Model

We use the approach proposed by Dorren (1987) to simulate the amplitude of the V, R, I magnitudes, and V−R, R−I and V−I color variations arising from the difference of fluxes between opposite stellar hemispheres owing to the presence of surface temperature inhomogeneities. We note that our model assumes a two temperature photosphere, however, this is a simplified approach, the photosphere of T Tauri stars being likely more complex. The stellar fluxes were determined by using the NextGen atmosphere models of Hauschildt et al. (1999) for solar metallicity and convolved with the passbands of the Bessel UBVRI system (Bessell 1990). Limb-darkening coefficients, different for the unperturbed and the perturbed photosphere, are taken from Diaz-Cordoves et al. (1995). We have computed the model magnitude and color variations for a grid of values of temperature and covering fraction assuming a two temperature photosphere. More specifically, the hotter zone might be an accretion spot or faculae zone or it might just be the photospheric temperature. Similarly, the cool zone might be a region of magnetically inhibited convection or it might just be the photospheric temperature. The photospheric stellar magnitude and colors are computed over the effective temperature range of the majority of our targets ($2800 < T_{eff}$ (K) < 3500) and for a range of surface gravities ($2.0 < \log g < 4.5$). The covering fraction was varied from 0.0 (no temperature inhomogeneities) to 1.0 (stars fully covered by temperature inhomogeneities) with a 0.1 increment, whereas the temperature of the surface inhomogeneities was varied in the range T_{eff}-1000 < T (K) < T_{eff}+1000 (see, e.g., Berdyugina 2005) with a 100 K increment. In our modeling approach, gravity-darkening effects are neglected by considering that these effects tend to cancel out when computing the flux difference between opposite hemispheres. We have plotted in Fig. 11 the results of our modeling. We note that the amplitude of both magnitude and color variations mostly depend on the filling factor of surface inhomogeneities, whereas slopes of the magnitude vs. color variation primarily depend on the temperature contrast between such inhomogeneities and the unspotted photosphere. The presence of regions either cooler or hotter determines magnitude and color variations whose slope Δ mag/Δ color is positive in both cases: cooler regions make the star fainter and redder (see the solid red lines marked by crosses in top right parts of Fig. 11), whereas hotter regions make the star brighter and bluer (both magnitude and color variations are negative as shown by solid blue lines marked by diamonds in the bottom left parts of Fig. 11). We find that the families of slope obtained by varying both the star's and the perturbed region's parameters fall within a limited range of values. The most interesting re-

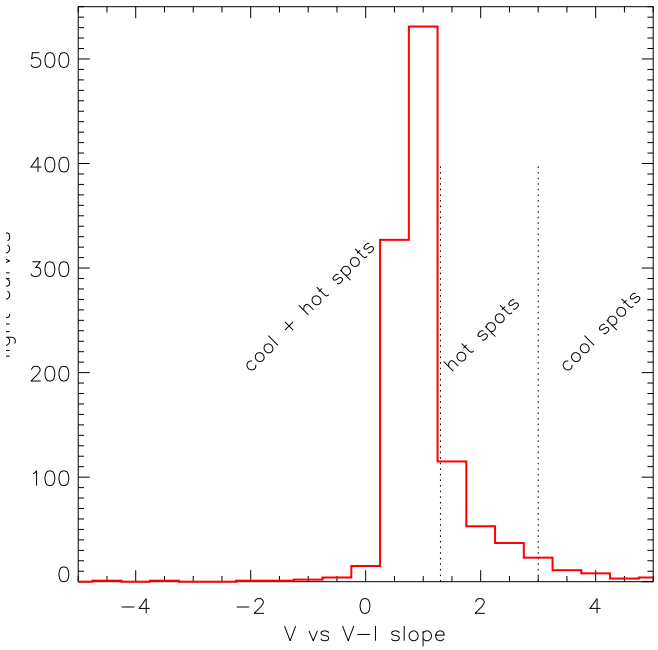

Figure 12. Distribution of V versus V−I slopes for known WTTS and CTTS in our sample. The vertical dashed line demarcate regions where according to our model, only cool spot (slope > 3) only hot spot ($1 <$ slope < 3) and a combination of cool and hot spots (slope < 1) may exist.

sult of our modeling is that slopes arising from the presence of only regions cooler ($3 < b < 5$) do not overlap with the slopes ($1.3 < b < 3$) arising from the presence of only regions hotter than the unperturbed photosphere. This allows us to use the V vs V−I color variation to investigate the nature of temperature inhomogeneities supposed to be present in the stellar surface. In our simulations we find that combinations of hot and cool regions simultaneously present on the same stellar hemisphere gives rise to slope values close to zero or negative.

To compare the model results with observations, we have computed linear regression, correlation analysis, and computed the relation slopes, their correlation coefficients, and the Pearson linear significance levels associated to the correlation coefficients for the V vs. V−I, R vs. R−I, and V vs. V−R magnitude-color relations. The results are listed in Table 4, where we list the following information: internal identification number (id), observation season (seas), mean HJD (HJD_{mean}), number of measurements in the I, R and V band (N_I, N_R, N_V) slope of the V vs. V−I relation (b_{VVI}) and correlation coefficient (r_{VVI}), slope of the R vs. R−I relation (b_{RRI}) and correlation coefficient (r_{RRI}), and slope of the V vs. V−R relation (b_{VVR}) and correlation coefficient (r_{VVR}), and slope of the R−I vs V−R (b_{RIVR}) and correlation coefficient (r_{RIVR}). We listed and used in the following analysis only those values for which the correlation has a confidence level $> 95\%$.

In Fig. 12 we plot the distribution of V vs. V−I slopes of all light curves. For a number of stars we have at our disposal up to 5 values of slopes determined from data collected in 5 observation seasons. We verified that the slope distribution obtained by considering all the light curves and the distribution obtained by using for each star the mean slope do not differ significantly. We also verified that no difference exists when we consider the whole sample of stars and a sub-sample of periodic stars. Finally we opted to consider the whole sample of stars (periodic plus non periodic) and the whole sample of light curve in order to have a better statistics.

We find that about 6% of light curves show a slope consistent with a variability arising from only cool spot (i.e. regions of magnetically inhibited convection); 18% of light curves show a slope with a variability arising from only hot spot (i.e. either accretion spot or faculae zones); whereas the majority (76%) show slopes consistent with a variability arising from the presence of both cool and hot spots. We remind that periodic clean and periodic dirty stars have a mean slope in the range 1-5–2.2, whereas non periodic stars, which are the majority, have smaller slopes. Moreover, bluer stars tend to have slopes more steep than redder stars.
This distribution provide us an interesting interpretation about the cause of variability, that is stars with either only cool or only hot spots have inhomogeneities patterns sufficiently stable to produce periodic light variations. One such case is represented by the ONC member V1481 Ori (Messina et al. 2016) whose photometric variability is dominated by hot spots, but its light curves were found to be so smooth that we could measure its rotation period in 15 out 16 seasons. On other hand when the variability arises from the combined effect of hot and cool spots then rotational modulation gives very scattered light curves and the stars are found to be non periodic.

6 AGE VERSUS MAGNITUDE DISPERSION

As mentioned earlier, the prime motivation of present study is not to determine absolute age of the ONC members under analysis, but to explore the impact of photometric variability on inferred stellar age and mass. Because of this, only one set of PMS evolutionary models well accomplished the aim.

We found that ages inferred by means of CMDs are not affected by photometric variability if stars exhibit a periodic photometric variability and the rotation phase magnitude dispersion is negligible with respect to the peak-to-peak light curve amplitude ($R \geqslant 2.5$, the so called 'clean periodic'). CMDs still provide a reliable estimate of the age also for periodic variables whose rotation phase magnitude dispersion becomes comparable to the peak-to-peak of light curve amplitude ($1 \leqslant R < 2.5$, the so called 'dirty periodic'). The inferred ages in the second case is found to be slightly older and the number of outliers (stars with ages significantly older than the average) reaches the 20%. However, the majority of stars in our sample are non periodic and ages inferred from CMDs become unreliable.

Very accurate knowledge of the photometric variability and the use of the magnitude-T_{eff} diagrams (to overcome

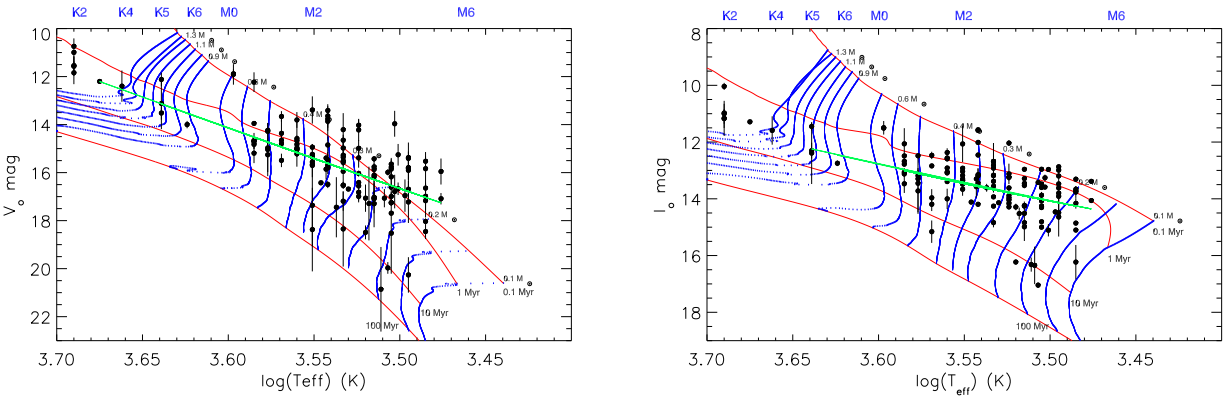

Figure 13. T_{eff}-V_0 (left panel) and T_{eff}-V_0 (right panel) diagrams of the ONC members under analysis for which the extinction is known. The black bullets represent the mean magnitudes (average magnitudes over a 5-yr long time series) whereas the vertical bars their range of variation (brightest minus faintest magnitudes). Red solid lines and blue dotted lines represents theoretical isochrones and mass tracks, respectively, from Siess et al. (2000).

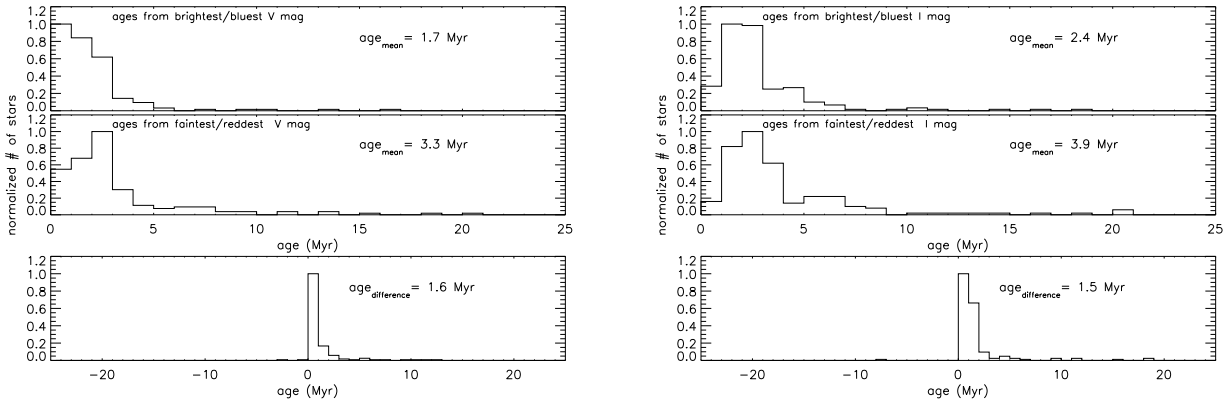
ages from brightest/bluest V mag
age_mean = 1.7 Myr
ages from faintest/reddest V mag
age_mean = 3.3 Myr
age_difference = 1.6 Myr
ages from brightest/bluest I mag
age_mean = 2.4 Myr
ages from faintest/reddest I mag
age_mean = 3.9 Myr
age_difference = 1.5 Myr
normalized # of stars
age (Myr)

Figure 14. Comparison between the mean magnitude dispersion in the T_{eff}-V_0 diagram and the amplitude of photometric variability (V band on left panel and I band on right panel). The magnitude dispersion is measured considering the residuals with respect to a 2nd order fit to the V_0 vs. T_{eff} distribution. The amplitude of photometric variability is measured considering the brightest minus faintest magnitudes over a time range of 5 yr.

uncertainties arising from the color variability) can be a robust tool to check the reality of age spread among the ONC members which has been debated by several authors (see, e.g., Reggiani et al. 2011). In the following, we estimate the age of the ONC members using the magnitude-T_{eff} diagrams, where the color is replaced by the spectroscopically measured effective temperature. We focus on a sub-sample of stars with known reddening that comprises periodic and non periodic members. In the left and right panels of Fig. 13, we plot the mean V_0 and I_0 magnitudes (averaged over the 5-yr time base) versus the effective temperatures taken from Hillenbrand (1997). The vertical bars indicate the observed maximum range of magnitude variation. Solid red and blue lines represent isochrones for the ages from 0.1 Myr to 100 Myr taken from Siess et al. (2000) and the evolutionary mass tracks in the range from 0.1 $M_\odot$ to 1.3 $M_\odot$. In Fig. 14, we plot the distributions of ages obtained considering the brightest/bluest magnitudes, faintest/reddest magnitudes, and the difference between the oldest and youngest ages for each star. We find that the average ONC age can be 1.7 Myr (brightest/bluest) to 3.3 Myr (faintest/reddest) and that the photometric variability can produce an average age difference of 2.5 Myr in the V band, and slightly larger in the I band.

In order to quantify the age dispersion, we measure the magnitude residuals with respect to a second order polynomial fit in the magnitude–T_{eff} diagram. The distribution of the residuals is plotted in Fig. 15 and represented with a heavy solid red line. We compare this distribution with the distribution of the amplitudes of photometric variability overplotted with an heavy dashed blue line. A gaussian fit to

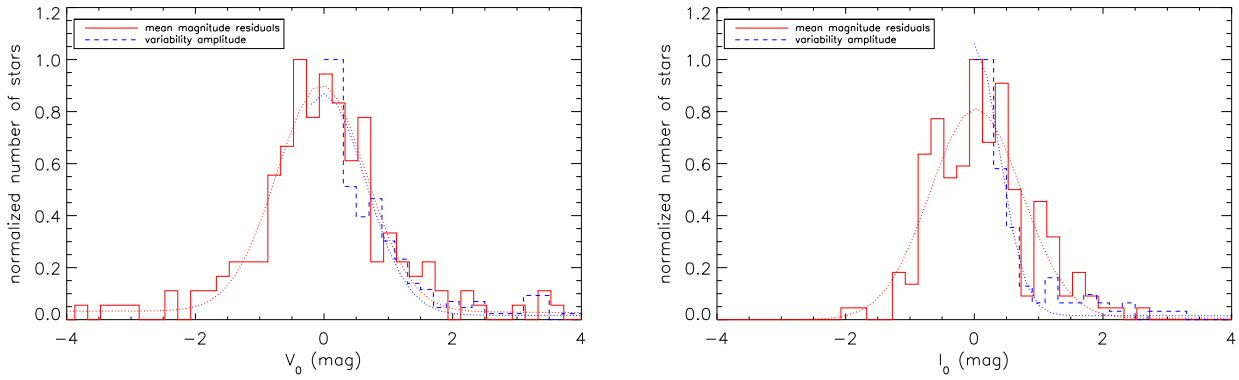

Figure 15. Comparison between the mean magnitude dispersion in the T_{eff}-V_0 diagram and the amplitude of photometric variability (V band on left panel and I band on right panel. The magnitude dispersion is measured considering the residuals with respect to a 2nd order fit to the V_0 vs. T_{eff} distribution. The amplitude of photometric variability is measured considering the brightest minus faintest magnitudes over a time rage of 5 yr.

the distributions (dotted red and blues lines, respectively) is used to measure the standard deviations of both distributions. We find that the distribution of magnitude residuals with respect to the polynomial fit has standard deviation σ = 0.70 mag, which is comparable to the standard deviation σ = 0.64 mag of the distribution of variability amplitudes. This new results derived from 5-yr V band photometry contradict with the conclusions made by Reggiani et al. (2011) that observational uncertainties and variability cause a luminosity dispersion significantly smaller than the apparent age dispersion. We find that that V band photometric variability level is large enough to mask any age spread and may be sole cause of the observed magnitude spread.

In the case of the I magnitude, we find that the distributions of magnitude residuals and amplitudes have, respectively, standard deviations σ = 0.71 mag and σ = 0.39 mag. Which indicates that the observed photometric variability can account for only a part (∼50%) of the observed magnitude spread in the magnitude-T_{eff} diagrams. To account to the remaining 50% spread, an intrinsic age distribution among the ONC member becomes essentials. The other possibility can be a radius dispersion among coeval members as consequence of non-uniform accretion at early stages, as suggested by Jeffries et al. (2011).

As mentioned several times, our statistics on the variability provides only a lower limit owing to the limited extension of the observation data base and the insufficient time resolution for transient phenomena. However, as shown in Fig 1, we do not expect that the variability amplitudes which we have measured are significantly underestimated. The inferred age dispersion, if not real, must be imputed to some other effects beside the variability.

7 CONCLUSIONS

We have monitored a sample of 346 members of the ONC in the V, R, and I bands for 5 consecutive years during 2003-2008. From analysis of the multi-band photometric time series data, we could measure variability in magnitude and color for all stars, which shows wide range of amplitudes. We measured the magnitude and colors maximum and minimum values, and the amplitude of variation, of each star in each observation season and in the full 5-yr timeseries. We find that the amplitude of variability in the V band is on average a factor two larger than in the I band. Moreover, the measured level of variability is found to increase as we extend the base line of observation. However, we find that within 2-3 consecutive years of monitoring, we could capture almost full range of the variability. The magnitude and color maximum and minimum values were used to infer mass and age of each star in color-magnitude diagrams using isochrones and evolutionary mass tracks from the models of Siess et al. (2000). We found that stars showing periodic and very smooth rotational light variations undergo magnitude and color variations with same slope as the theoretical isochrones. As a consequence, the variability does not affect their inferred mass and age. On other hand, stars showing periodic but very scattered rotational light variations or non periodic stars undergo magnitude and color variations with a slope smaller than that of theoretical isochrones and, consequently, appear older and more massive. Modeling the slope of the magnitude versus color variations by following the the methodology given by Dorren (1987), we find that the use of V vs. V−I variations allows to infer if the photometric variability is caused by zones hotter, zones cooler than the unperturbed photosphere, or a combination of both. We find the majority of stars to fall in the last category. Using magnitude-T_{eff} diagrams, instead of color-magnitude diagrams where color is affected by significant variability, and the PMS models of Siess et al. (2000), we find that for V band the apparent age spread can be mostly accounted by the photometric variability. In other words the age dispersion in the ONC is completely masked by the V-band variability. On the contrary, the amplitudes of variability in the I band have a dispersion that is a factor two smaller than the I mean magnitude dispersion. Therefore, I-band variability can take account of only 50% of magnitude spread in the

HR diagram. The remaining 50% spread requires a different explanation and may be due to age dispersion within ONC members which we find to be of about 1.5 Myr.

ACKNOWLEDGEMENTS

Research on stellar activity at INAF- Catania Astrophysical Observatory is supported by MIUR (Ministero dell'Istruzione, dell'Universitá e della Ricerca). The work is based on data collected at the Indian Institute of Astrophysics (IIA). The extensive use of the SIMBAD and ADS databases operated by the CDS centre, Strasbourg, France, is gratefully acknowledged. We thank the referee, Prof. W. Herbst, for valuable comments.

REFERENCES

Berdyugina S. V., 2005, Living Reviews in Solar Physics, 2, 8
Bessell M. S., 1990, PASP, 102, 1181
Da Rio N., Robberto M., Soderblom D. R., Panagia N., Hillenbrand L. A., Palla F., Stassun K. G., 2010, ApJ, 722, 1092
Diaz-Cordoves J., Claret A., Gimenez A., 1995, A&AS, 110, 329
Dorren J. D., 1987, ApJ, 320, 756
Grankin K. N., Melnikov S. Y., Bouvier J., Herbst W., Shevchenko V. S., 2007, A&A, 461, 183
Grankin K. N., Bouvier J., Herbst W., Melnikov S. Y., 2008, A&A, 479, 827
Hauschildt P. H., Allard F., Baron E., 1999, ApJ, 512, 377
Herbst W., Rhode K. L., Hillenbrand L. A., Curran G., 2000, AJ, 119, 261
Herbst W., Bailer-Jones C. A. L., Mundt R., Meisenheimer K., Wackermann R., 2002, A&A, 396, 513
Hillenbrand L. A., 1997, AJ, 113, 1733
Jeffries R. D., Littlefair S. P., Naylor T., Mayne N. J., 2011, MNRAS, 418, 1948
Messina S., 2008, A&A, 480, 495
Messina S., Rodonò M., Guinan E. F., 2001, A&A, 366, 215
Messina S., Rodonò M., Cutispoto G., 2004, Astronomische Nachrichten, 325, 660
Messina S., Desidera S., Turatto M., Lanzafame A. C., Guinan E. F., 2010, A&A, 520, A15
Messina S., Desidera S., Lanzafame A. C., Turatto M., Guinan E. F., 2011, A&A, 532, A10
Messina S., Parihar P., Biazzo K., Lanza A. F., Distefano E., Melo C. H. F., Bradstreet D. H., Herbst W., 2016, MNRAS, 457, 3372
Oláh K., et al., 2009, A&A, 501, 703
Parihar P., Messina S., Distefano E., Shantikumar N. S., Medhi B. J., 2009, MNRAS, 400, 603
Reggiani M., Robberto M., Da Rio N., Meyer M. R., Soderblom D. R., Ricci L., 2011, A&A, 534, A83
Rodríguez-Ledesma M. V., Mundt R., Eislöffel J., 2009, A&A, 502, 883
Siess L., Dufour E., Forestini M., 2000, A&A, 358, 593
Stassun K. G., Mathieu R. D., Mazeh T., Vrba F. J., 1999, AJ, 117, 2941

APPENDIX A: MEASUREMENT OF LIGHT CURVE AMPLITUDE

As described earlier, to measure the amplitude of the clean periodic light curves we use the amplitude of the sinusoidal fit. This ensures that there is no overestimation of amplitude due to residual outliers. Whereas, in case of dirty periodic stars, the amplitude of the sinusoidal fit tends to underestimate the true amplitude of the light curve. Therefore, for the dirty periodic and irregular variables we estimate the brightest and faintest magnitudes as well as the amplitude by following two different approaches. In the first approach we derive the relation between the light curve amplitude and its root mean square (RMS) using the sample of clean stars. Thereafter, we apply this relation to estimate the amplitude of the light curve of dirty stars by using the computed rms. In Fig. A1 we have shown the plots of amplitude versus RMS for different bands and colors, whereas fitting results are given in the Table A1. In each panel we report the correlation coefficient, its significance level according to the Person statistical test, and the slope of a linear fit. We found very tight correlation between amplitude and RMS and this relation enables us to derive the average light and color curve amplitudes from the measurement of their RMS for the stars which have either no smooth light curves or having light curves but very scattered ('dirty' periodic sample). To minimize the effect of outliers on the determination of RMS, we select only light curves which have at least 30 measurements.

Another approach is to consider the, e.g., 20% brightest and 20% faintest magnitudes of a 'dirty' light curve and to use their average values as measurement of the brightest and faintest magnitude. Both approaches can be tested with clean light curves which has got known amplitudes of variability. That means we can compare amplitudes derived from direct sinusoidal fitting to amplitudes computed from RMS (first approach) and/or the amplitudes obtained by averaging the extreme bands of the magnitude distribution (second approach).

We find that the amplitudes derived from both approaches are essentially similar, i.e, their difference gives zero mean value with a dispersion of about 0.01 mag. As expected, we find that increase in magnitude of phase dispersion of the light curve (from clean to dirty) deliberately makes the amplitude of the sinusoidal fit to be smaller than the amplitude derived from either the first or the second approach.

We have also made a comparison between the distribution of RMS in the clean and dirty samples to further investigate whether they statistically belong to same or to different distributions. The confidence level that RMS distributions of light curves in the 'dirty' and 'clean' samples come from the same parent distribution is computed with Kolmogorov-Smirnov (KS) tests. We find that it is larger than 99.9% in the I band, 53% in the R and 13% in the V band. Although the R band distribution is based on only 41 against the 243 values of V band, its confidence level is much higher. In case of V and R bands we find that distributions are quite different which appears not due to the poor statistics (smaller sample), but seems to be an effect of variability phenomena not related to rotational modulation. A comparison between color RMS distributions reflects similar results: R−I color has RMS in the clean and dirty samples more similar than V−R and V−I (KS_{ri}=83%, KS_{vi}=35%,

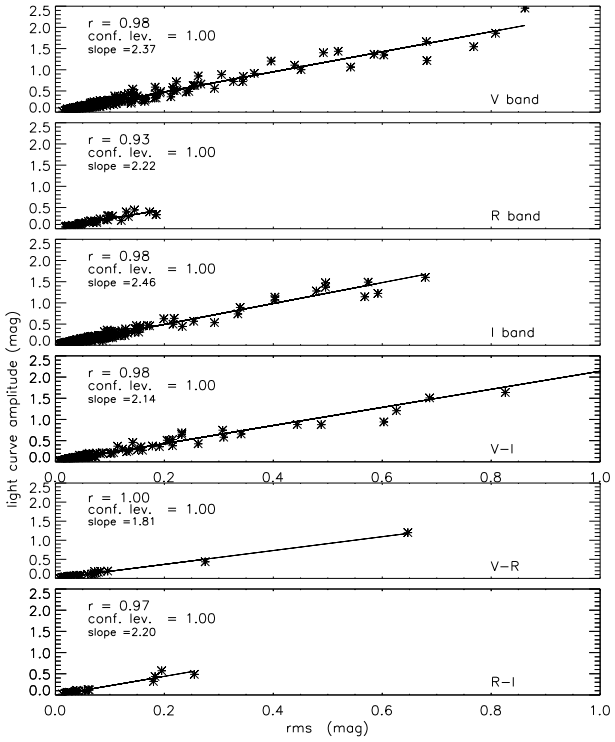

Figure A1. Distributions of light and color curve amplitudes versus RMS. Solid lines are the linear fits. Labels report the correlation coefficient(r), the confidence level from Pearson test, and slope of the linear fits.

Table A1. Average ratio between the amplitude and RMS of light and color curves..

Band	amplitude/rms	# light curve
V	2.37 ±0.03	235
R	2.22 ±0.14	41
V	2.46 ±0.02	350
V−I	2.14 ± 0.03	350
V−R	1.81 ± 0.03	27
R−I	2.30 ± 0.12	25

KS_{vr}=21%). Based on the results of KS tests, we transform dirty RMS into amplitude values only for I and R bands and R−I color. The V band amplitudes derived from RMS may be little over estimated, however that gives us a possibility to investigate the impact of magnitude and color variations in CMDs on a much larger stellar sample. We could verify that no dependence of the ratio on the star's brightness exists, since the photometric accuracy equally affect both the light curve amplitude and the dispersion. To summarize, amplitudes of periodic clean light curve can be derived from sinusoid fit, RMS and percentiles. Amplitudes of non periodic or dirty light curves are better estimated from percentile, since sinusoid fit underestimated whereas RMS method overestimate. To get homogeneous estimated we have used the percentile for all the light curves.